https://doi.org/10.5194/egusphere-2023-659
Preprint. Discussion started: 5 May 2023


# Technical Note: Monitoring discharge of mountain streams by retrieving image features with deep learning

Chenqi Fang[1], Genyu Yuan[1], Ziying Zheng[1], Qirui Zhong[1], Kai Duan[1*]

[1] *School of Civil Engineering, Sun Yat-Sen University, Guangzhou, China*

*Corresponding author, E-mail: duank6@mail.sysu.edu.cn

https://doi.org/10.5194/egusphere-2023-659
Preprint. Discussion started: 5 May 2023


## Abstract

Traditional discharge monitoring usually relies on measuring flow velocity and cross-section area with various velocimeters or remote-sensing approaches. However, the topography of mountain streams in remote sites largely hinders the applicability of velocity-area methods. We here present a method to continuously monitor mountain stream discharge using a low-cost commercial camera and deep learning algorithm. A procedure of automated image categorization and discharge classification was developed to extract information on flow patterns and volumes from high-frequency red–green–blue (RGB) images with deep convolutional neural networks (CNNs). The method was tested at a small, steep, natural stream reach in southern China. Reference discharge data was acquired from a V-shaped weir and ultrasonic flowmeter installed a few meters downstream of the camera system. Results show that the discharge-relevant stream features implicitly embedded in RGB information can be effectively recognized and retrieved by CNN to achieve satisfactory accuracy in discharge measurement. Coupling CNN and traditional machine learning models (e.g., support vector machine and random forest) can potentially synthesize individual models' diverse merits and improve generalization performance. Besides, proper image pre-processing and categorization are critical for enhancing the robustness and applicability of the method under environmental disturbances (e.g., weather and vegetation on river banks). Our study highlights the usefulness of deep learning in analyzing complex flow images and tracking flow changes over time, which provides a reliable and flexible alternative

apparatus for continuous discharge monitoring of rocky mountain streams.

**Keywords**:

Discharge monitoring; Mountain streams; Deep learning; Machine learning; Image categorization

# 1 Introduction

Continuous discharge data is critical for hydrological model development and flood forecast (Mcmillan et al., 2010; Clarke, 1999), water resources management (Council, 2004), and aquatic ecosystem health assessment (Carlisle et al., 2017). Traditional discharge monitoring relies on stream gauges that convert water level to discharge with an established stage-discharge curve, or information on stable cross-sections and flow velocity obtained from flow velocimeters such as acoustic doppler current profiler (ADCP) and ultrasonic defectoscope (Kasuga et al., 2003). However, these approaches require significant investment on the implementation of equipments, training of personnel with expertise, and constant maintenance (Fujita et al., 2007; Czuba et al., 2017; Yorke and Oberg, 2002). Besides, the performance of transducers and velocimeters is usually susceptible to sediments and floating debris, particularly in flooding seasons (Hannah et al., 2011). Consequently, large temporal gaps remain in many discharge records across the world despite of the growing demand on data (Davids et al., 2019; Royem et al., 2012). Spatially, flow monitoring of downstream river sections has been assigned to a higher priority due to the concerns on water supply and flood control, leading to an acute shortage of discharge data in mountain streams

https://doi.org/10.5194/egusphere-2023-659
Preprint. Discussion started: 5 May 2023


and headwater catchments (Deweber et al., 2014).

To overcome the limitations of traditional methods, a few image-based approaches have been introduced into water stage, flow velocity, and discharge measurement in rivers (Noto et al., 2022; Leduc et al., 2018). Image-based (Leduc et al., 2018; Noto et al., 2022) approaches rely only on the acquisition of digital images of streams from inexpensive commercial cameras and thus have been a promising alternative for continuous, noninvasive, and low-cost streamflow monitoring. The two most commonly used approaches include large-scale particle image velocimetry (LSPIV) and particle tracking velocimetry (PTV). LSPIV (Fujita et al., 1998) is based on a high-speed cross-correlation scheme between an interrogation area (IA) in a first image and IAs within a search region (SR) in a second image. The technique has been proved effective in monitoring low-velocity and shallow-depth flow fields (Tauro et al., 2018). However, it performs poorly in mapping velocity fields in high resolution when there is a lacking of seeds on the water surface because the algorithm obtains the average speed of each SR (Tauro et al., 2017). Compared to LSPIV, PTV was designed for low seeding density flows, focusing on particle tracking instead of recognition. The PTV approach does not require assumptions on flow steadiness nor the relative position of neighbor particles (Tauro et al., 2018). Several algorithms have been developed for PTV analysis, such as space-time image velocimetry (STIV) and optical tracking velocimetry (OTV), overcoming the over-dependence on natural particles' shape and size (Tauro et al., 2018; Tsubaki, 2017). STIV evaluates surface flow velocity by analyzing a texture angle within a variation of brightness or color on the water surface,

https://doi.org/10.5194/egusphere-2023-659
Preprint. Discussion started: 5 May 2023


while OTV combines automatic feature detection, Lucas-Kanade tracking algorithm and track-based filtering methods to estimate subpixel displacements (Karvonen, 2016; Fujita et al., 2007). Existing image-based discharge measurement methods all use the velocity-area method to indirectly deduce discharge after identifying stage and average (Davids et al., 2019; Herzog et al., 2022; Leduc et al., 2018; Tsubaki, 2017) velocity. The average velocity in a cross-section is estimated with surface velocity derived from natural or artificial seeds on water surface and pre-defined empirical relationships between the surface velocity and average velocity. The velocity-area method relies on a stable relationship between stage and cross-sectional area, and needs to take velocity extrapolations to the edges and vertical distributions throughout the cross-section into account (Le Coz et al., 2012). However, it is difficult to identify the water stage and vertical characteristics of mountain streams due to the steep, narrow, and highly heterogeneous cross-sections. The applicability of PIV and PTV approaches is largely hindered by such topography.

In this study, we propose a novel mountain stream discharge monitoring method using a low-cost commercial camera and deep learning models. Automated image categorization and pre-processing procedures were developed for processing high-frequency red–green–blue (RGB) images, and then the convolutional neural network was used to extract information on flow patterns from RGB matrixes and establish empirical relationships with the classification probabilities of discharge volumes. We hypothesize that (1) the features of mountain streams (e.g., coverage of water surface, flow direction, flow velocity) embedded in RGB images can be recognized by suitable

https://doi.org/10.5194/egusphere-2023-659
Preprint. Discussion started: 5 May 2023


deep learning approaches to achieve effective discharge monitoring, and (2) proper image pre-processing and categorization can improve accuracy of image-based discharge monitoring of mountain streams. A rocky mountain stream of a headwater catchment in tropical southern China was used as a study site to test our hypotheses.

# 2 Methods

## 2.1 Site and field setting

The study site is located on a small, steep, rocky reach of a stream in the Zhuhai Campus of Sun Yat-sen University, China (22°20′58″ N, 113°34′29″ E). The site elevation is 13 m above sea level and about 2 km away from the Lingding Yang of South China Sea. The stream flow is mainly controlled by rainfall in the upstream drainage area. Water stage and flow velocity increase rapidly during East Asian summer monsoon rainfalls and fluctuate with synoptic weather conditions on dry days.

The main objective of the study was to test the applicability of deep-learning based image processing approaches in capturing the flow characteristics and discharge volumes in the daily flow cycle in this mountain stream. We selected a straight, single-thread reach for the gauging location, and set up a Hikvision camera on the left bank of the stream to collect flow images (**Fig. 1**). Discharge data monitored by a weir about 8 m downstream of the camera was used for model training and validation. The camera was installed 3 m above the ground, facing the surface of the stream almost vertically. The entire stream width is visible in the images. The camera was equipped with a 150W

https://doi.org/10.5194/egusphere-2023-659
Preprint. Discussion started: 5 May 2023


solar panel and 80AH lithium battery, enabling the camera to work continuously for 80 hours without external power on rainy days. The camera supports the wireless transmission of video data to the server.

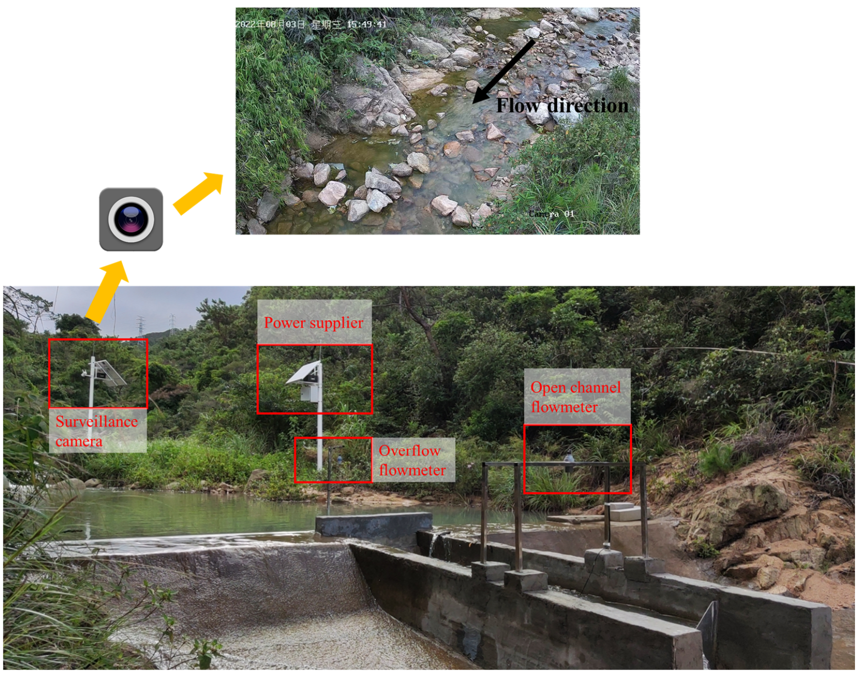


**Figure 1.** Camera setup. The camera is set on the left bank of the stream, about 3 m above the water surface, and 8 m upstream of a gauging weir.

## 2.2 Data

The flat V-shaped weir downstream of the camera monitors discharge with an open channel flowmeter and an overflow flowmeter. The flowmeters measure water levels in the channel and in front of the weir with ultrasonic sensors and calculate real-time discharge at the time step of two minutes by a semi-empirical equation suggested by

https://doi.org/10.5194/egusphere-2023-659
Preprint. Discussion started: 5 May 2023


the State Bureau of Technical Supervision of China (www.chinesestandard.net), as

$$Q = \frac{8}{15} C_e \tan\frac{\theta}{2} \sqrt{2g} h_e^{\frac{5}{2}} \tag{1}$$

where $Q$ is the discharge of stream, $\theta$ is the angle of triangular weir, $g$ is acceleration of gravity, $h_e$ is the height of the triangle barrier from the bottom, $C_e$ is an empirical coefficient.

We collected the discharge data of the weir and its corresponding stream videos during daylight (07:00-19:00 UTC+8) from July 20$^{th}$ to September 27$^{th}$, 2022. The raw video resolution was 2560×1440 pixels with a refresh rate of 50 Hz. Images were extracted from the videos at the 5- minute interval to avoid excessive similarity between adjacent images. A total of 7,757 image samples labeled with 37 discharge values between 0.014 and 0.050 $m^3/s$ were collected for model testing.

## 2.3 Image processing

### 2.3.1 Image categorization

Environmental disturbances such as illumination and shadow can seriously interfere with the extraction of effective image features of mountain streams, such as boundaries of water surface and textures of flow lines (Gershon et al., 1986; Herzog et al., 2022). Although researchers have proposed methods to eliminate shadows (Finlayson et al., 2002), the treatment effect in some complex environments, such as plant shadows and boulders distributed on mountain streams, is not always satisfactory.

Frequently observed disturbances on images include: (1) shadows in the target stream region due to plants blocking direct sunlight; (2) image noise due to raindrops attached

https://doi.org/10.5194/egusphere-2023-659
Preprint. Discussion started: 5 May 2023


to the camera lens on rainy days; (3) the lack of light leading to low brightness and contrast of the image; (4) overexposure of image due to light reflection of the water surface (around 16:00 UTC+8 in this case). Taking these factors into consideration, we divided all image samples into six categories, including "Good quality", "Raindrops", "Middle shadow", "Below shadow", "Water reflection", and "Dark" (**Fig. 2**). "Good quality" contains image samples without obvious noise or shadow. All the other images lose some feature information due to noise, shadows, reflections, or dim lighting. To ensure the model performance under different environmental conditions, we designed an automated categorization procedure to screen the raw images and exclude the "Raindrops" and "Dark" samples from model training. The procedure categorizes images by comparing the feature values of brightness or saturation in particular test areas to predefine thresholds under different conditions (see **Section 3.2)**.

https://doi.org/10.5194/egusphere-2023-659
Preprint. Discussion started: 5 May 2023


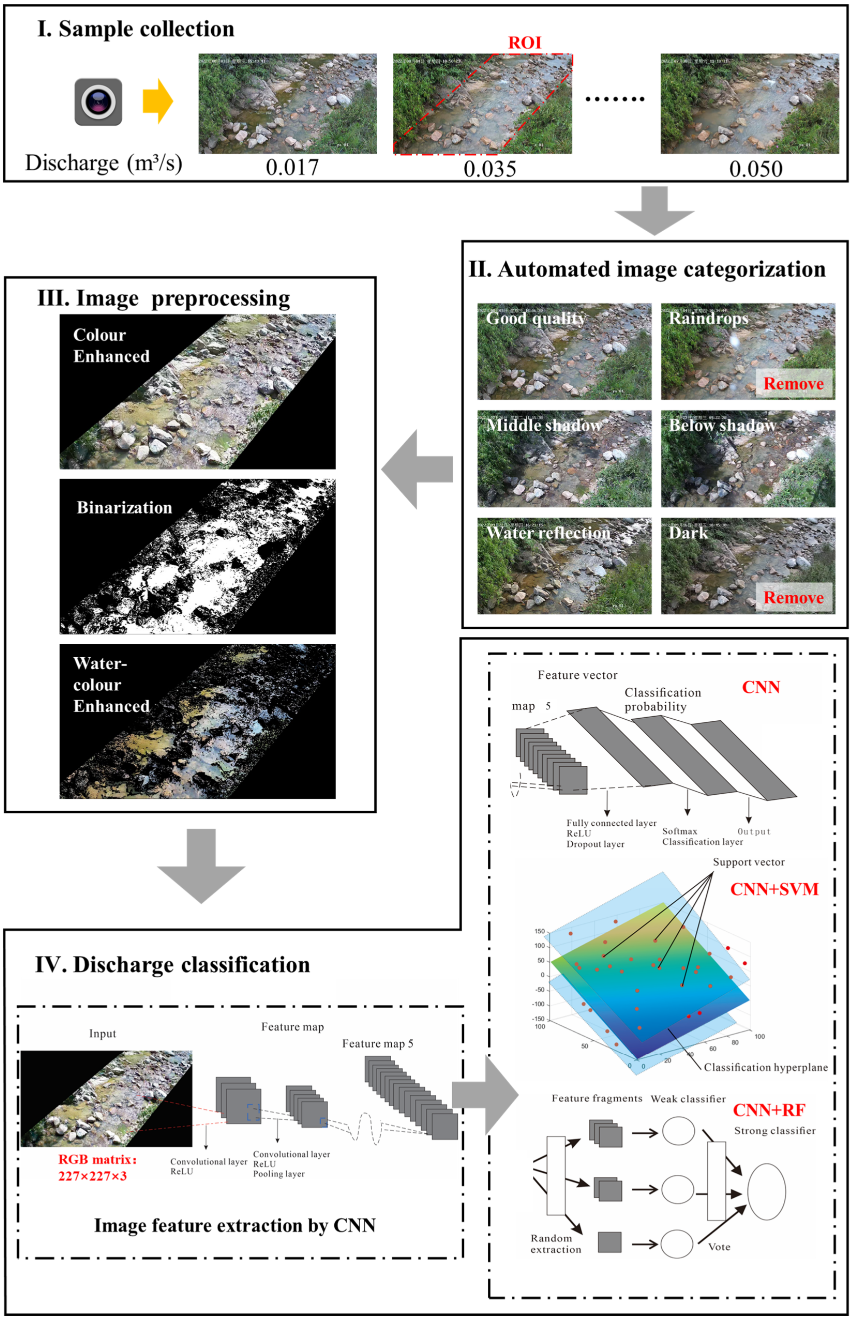


159

160 **Figure 2.** Flowchart of image processing and discharge monitoring.

161

https://doi.org/10.5194/egusphere-2023-659
Preprint. Discussion started: 5 May 2023


#### 2.3.2 Color enhancement

In order to highlight the stream features embedded in the images and avoid image information redundancy, we compared three commonly used color enhancement approaches to process the image samples.

**(1) Color Enhanced.** A dynamic histogram equalization technique (Abdullah-Al-Wadud et al., 2007; Cheng and Shi, 2004) was used to enhance contrast and emphasize stream features. First, vegetation areas on both sides of the stream were cropped and filled with black. Then, histogram equalization was used to enhance the contrast between light and dark, i.e., brighten the bubbles, swirls, ripples, splashes, water coverage, etc., and darken the bottom stones and reflections in the water.

**(2) Binarization.** Binarization of image information can decrease the computational load and enable the utilization of simplified methods compared to 256 levels of grey-scale or RGB color information (Sauvola and Pietikäinen, 2000; Finlayson et al., 2002). In this case, the RGB and HSB (Hue, Saturation, Brightness) information extracted from images suggests that the brightness of the stream water under daylight ranges from 0.2 to 0.7, and the values of three color components follow:

$$R(x,y)+G(x,y)+B(x,y)>350 \tag{2}$$

Where $R(x,y)$, $G(x,y)$ and $B(x,y)$ respectively represent the red, green, and blue color values of the pixel (x, y). The original image was transformed into a binary image by assigning the values of "1" and "0" to the pixels within and out of the water body, respectively.

**(3) Water-color Enhanced.** Considering that water-color features may carry some

https://doi.org/10.5194/egusphere-2023-659
Preprint. Discussion started: 5 May 2023


useful information on discharge (Kim et al., 2019), we tested a new pre-processing method combining the two approaches above. The RGB information of the original image within the water body areas was kept unchanged, while the non-water body areas were filled with black color. Then, the water body areas were further enhanced with the histogram equalization method to highlight the edge transition between the water body and the background (Abdullah-Al-Wadud et al., 2007).

#### 2.3.3 Image denoising

Images pre-processed by all of three approaches still contain large amounts of noise due to environmental disturbances and edge oversharpening caused by image contrast enhancement (Herzog et al., 2022). Therefore, the wavelet transform (Zhang, 2019) was adopted to denoise the image samples. We chose a compromise threshold between hard and soft thresholds as the threshold function (Chang et al.). When the wavelet coefficient is greater than or equal to the threshold, a compromise coefficient $\alpha$ ranging from 0 to 1 is added before the threshold to achieve a smooth transition from hard to soft thresholds,as

$$\lambda = \frac{median(d_j(k))}{0.6745} \times \sqrt{2\log(M \times N)} \tag{3}$$

$$\omega_\lambda = \begin{cases} [sign(\omega)](|\omega| - \alpha\lambda), |\omega| \geq \lambda \\ 0, |\omega| \geq \lambda \end{cases} \tag{4}$$

where $j$ is the scale of wavelet decomposition, $d_j(k)$ is the coefficient of wavelet decomposition, $M$ and $N$ are the length and width of images, $\omega$ is the wavelet coefficient, $\lambda$ is the set threshold, and $sign$ is the sign function. In this case, $M$×$N$=2560×1440, $\alpha$=0.5.

https://doi.org/10.5194/egusphere-2023-659
Preprint. Discussion started: 5 May 2023


## 2.4 Algorithms of discharge estimation

We used three algorithms to establish discharge classification models (**Fig. 2**), including convolutional neural network (CNN), support vector machine (SVM), and random forest (RF). The data of the RGB color matrix derived from pre-processed images was used as model inputs. SVM and RF were coupled with CNN to explore the potential merits of traditional machine learning algorithms in improving the accuracy and efficiency of CNN-based discharge classifiers.

### 2.4.1 Convolutional Neural Network (CNN)

Deep convolutional neural network allows computational models composed of multiple processing layers to learn representations of data with multiple levels of abstraction, which have brought breakthroughs in processing images, video, speech, and audio (Lecun et al., 2015). The AlexNet architecture (Krizhevsky et al., 2017) was used to construct our model. Parameters of the semantic layer of the model were calibrated to achieve feature extraction and classification of stream images. The image size was first rescaled from 2560×1440 to 227×227 to facilitate the migration of trained AlexNet. A 227×227×3 (length×width×color) matrix was retrieved from each image as the model input. There were five built-in convolutional layers, using a 3×3 convolution kernel and a 3×3 pooled kernel. We replaced the last three layers of AlexNet with a full-connection layer, a softmax layer, and a classification layer, leaving all other layers intact. The parameters of the full-connection layer were set according to the number of selected discharge values. The ReLU function was used as the convolutional layer activation

https://doi.org/10.5194/egusphere-2023-659
Preprint. Discussion started: 5 May 2023


function to extract and pass on the water coverage features. The SoftMax function was the activation function of the output layer, and the extracted feature vectors were compressed under each discharge label. The probability that a stream image falls into a discharge label was calculated as

$$P(y|x) = \frac{e^{h(x,y_i)}}{\sum_{i=1}^{n} e^{h(x,y_i)}} \tag{5}$$

where $x$ is the feature vector extracted by CNN, $y$ is the discharge label, $n$ is the number of labels, $h(x, y_i)$ is the linear connectivity function. The training method for CNN was stochastic gradient descent with momentum, with 15 samples in small batches, a maximum number of rounds of 10, and an initial learning rate of 0.00005. The samples were shuffled in every epoch.

#### 2.4.2 Convolutional Neural Network coupled with Support Vector Machine (CNN+SVM)

SVM is a machine learning method based on structural risk minimization and Vapnik–Chervonenkis (VC) dimension theory (Cortes and Vapnik, 1995). It has been widely used in image processing, pattern recognition, fault diagnosis, prediction and classification (Burges, 1998), which can help to capture key samples and eliminate redundant samples by finding the optimal hyperplane. Compared with neural networks, which rely on large training samples and tend to fall into local optima, SVM can achieve global optima with a simpler model structure (Hanczar et al., 2010; Matykiewicz and Pestian, 2012). However, the SVM-based classifier requires manual input of image features. Therefore, we coupled CNN and SVM to achieve automatic discharge

https://doi.org/10.5194/egusphere-2023-659
Preprint. Discussion started: 5 May 2023


classification. Image features extracted by CNN (i.e., the output of the 5th CNN pooling layer) were fed into SVM classifiers to calculate discharge.

**2.4.3 Convolutional Neural Network coupled with Random Forest (CNN+RF)**

RF (Ho, 1995) is a flexible machine-learning algorithm that combines the output of multiple decision trees to reach a single result. Each decision tree depends on the values of a random vector sampled independently and with the same distribution for all trees in the forest (Breiman, 2001; Panda et al., 2009). It is an integrated algorithm of the Bagging type (Aslam et al., 2007) that combines multiple weaker classifiers, and the final result is obtained by voting or averaging to improve accuracy and generalization performance. We here used an RF with 350 decision trees and five decision leaves. The coupling method of CNN+RF is similar to CNN+SVM, using the same pooling outputs of CNN as the inputs of RF discharge classifiers.

# 3 Results

## 3.1 Correlation between color information and discharge

The unstructured image data of mountain streams implicitly contain many stream features relevant to discharge, such as the width and depth of streams, the coverage of water surface, and spatial distributions of flow direction and flow velocity. CNN has been widely used in various classification and regression problems for its capability in recognizing the features of interest from images (Krizhevsky et al., 2017). In this study, we attempted to achieve discharge monitoring by establishing empirical relationships

https://doi.org/10.5194/egusphere-2023-659
Preprint. Discussion started: 5 May 2023


between the RGB color information of the water body and the discharge volumes. We first explored the correlation between the combination of R/G/B values in the region of interest (ROI, see **Fig. 2**) and discharge conditions. Traversing the common algebraic combinations of the three colors, we found that $-\bar{R} + 7.5\bar{G} - 6.5\bar{B}$ ($\bar{R}$, $\bar{G}$, $\bar{B}$ are the mean values of red, green and blue channels of an image, respectively) had a spearman correlation coefficient of 0.67 with discharge (p-value < 0.01), indicating that the discharge is significantly correlated with the color combination value at the 99% confidence level (**Fig. 3**). Such result suggests that discharge conditions are embedded in RGB information of mountain streams to some extent, which could be further retrieved and refined by CNN models.

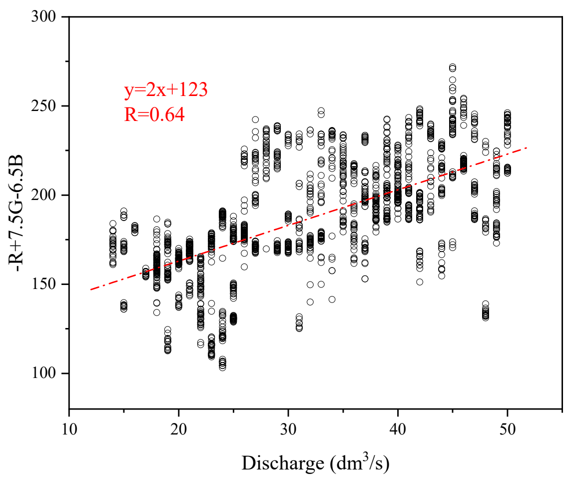


**Figure 3.** Correlation between RGB color values and corresponding discharges.

## 3.2 Automated image categorization

We selected four areas in the image as the detection areas for the categorization procedure (**Fig. 4a**). It was found that the upper and lower shadows in the target stream

https://doi.org/10.5194/egusphere-2023-659
Preprint. Discussion started: 5 May 2023


section mainly appeared in Area 3 and Area 1&2, respectively. Disturbance of water surface reflection was mostly found in Area 4. The thresholds of saturation or brightness in the four detection areas for image categorization were determined manually by comparing image samples under different conditions. The procedure of automated image categorization includes four steps (**Fig. 5**). First, "Dark" images (**Fig. 4f-2**) were identified when the standard deviation of the brightness or saturation of the full image was less than 0.2. "Raindrops" images (**Fig. 4f-3**) were identified when the mean difference of the saturation or brightness of the image was greater than 35% compared to the "Good quality" images (**Fig. 4f-1**). These two types of images were excluded from the training samples. Then, "Below shadow" (**Fig. 4b-2**; **Fig. 4c-2)** and "Middle shadow" images (**Fig. 4d-2**) were identified when the brightness value with the largest number of pixels in Area 1&2 and Area 3 was less than 0.3 and 0.4, respectively. Last, "Water reflection" images were identified when the number of pixels at the brightness value of 0.98 in Area 4 exceeded 1300 (**Fig. 4e-2**). The other charts in **Fig. 4** show the saturation and brightness distributions in each detection area derived from a typical "Good quality" image.

https://doi.org/10.5194/egusphere-2023-659
Preprint. Discussion started: 5 May 2023


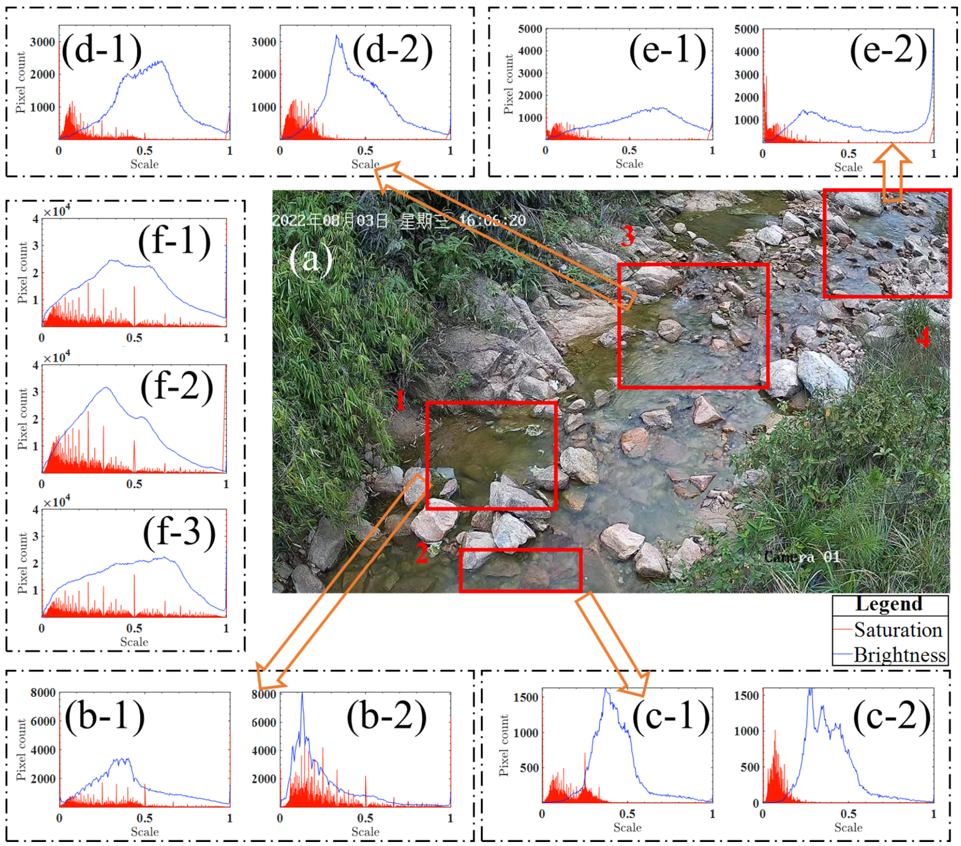


**Figure 4.** Comparison of saturation and brightness distributions in the four detection areas under different environmental conditions. The horizontal axis is the interval range (0-1) of saturation and brightness in HSB space. The vertical axis indicates the number of pixels under a certain saturation or brightness value.

https://doi.org/10.5194/egusphere-2023-659
Preprint. Discussion started: 5 May 2023


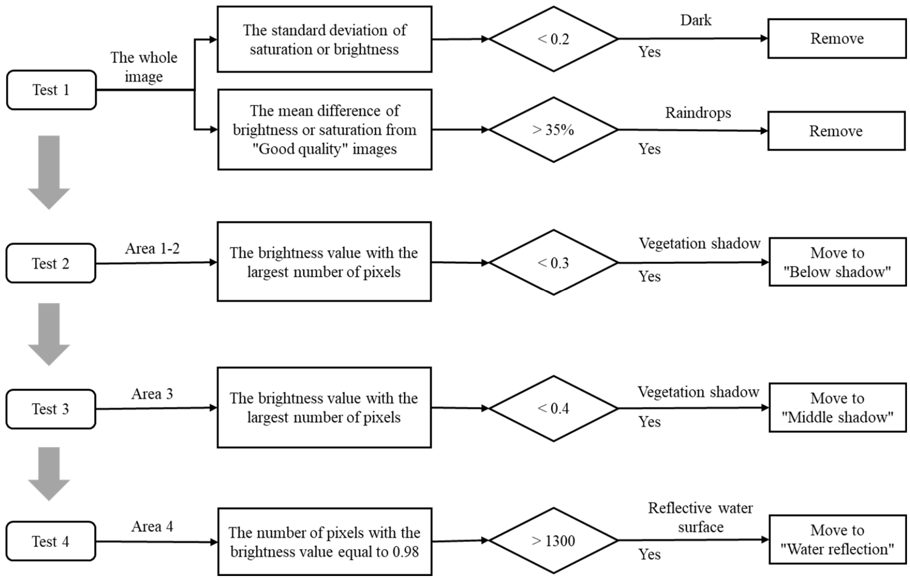


**Figure 5.** Procedure of automated image categorization.

## 3.3 Model training and validation

We selected 100 stream images corresponding to each discharge volume for model training and validation. The databases of "Good quality", "Middle shadow", "Below shadow", and "Water reflection" were sampled in the ratio of 7:1:1:1 to ensure the representation of different environmental conditions. The samples were distributed evenly in each discharge interval to enhance model performance on high and low flows.

### 3.3.1 Effectiveness of image categorization

Most of the previous image-based studies only selected unblemished images for discharge or velocity monitoring, which resulted in poor model performance under environmental disturbances. (Chapman et al., 2020; Herzog et al., 2022; Leduc et al.,

https://doi.org/10.5194/egusphere-2023-659
Preprint. Discussion started: 5 May 2023


2018) In this study, we also included samples under the influence of vegetation shadows and water reflection for model training. **Fig. 6** demonstrates the difference in accuracy of monitoring discharge by the defective images, using two sets of models trained with only "Good quality" images and samples filtered by automated image categorization, respectively. Results derived from the three discharge classification models and three color-enhancing methods consistently suggest that the procedure of automated image categorization can significantly improve model performance in apprehending defective images. Classification accuracy of the models trained with only "Good quality" samples staggered between 11.8%-18.7%, while the accuracy of the models trained after automated image categorization was higher than 79.0% (79.0%-97.4%) regardless of the choices of color processing method and deep learning model. The average difference in accuracy between the two sets of training samples reached 73.9%. The proportionate inclusion of defective images with vegetation shadow and water surface reflection enhances the anti-interference ability of the models in complex environments.

https://doi.org/10.5194/egusphere-2023-659
Preprint. Discussion started: 5 May 2023


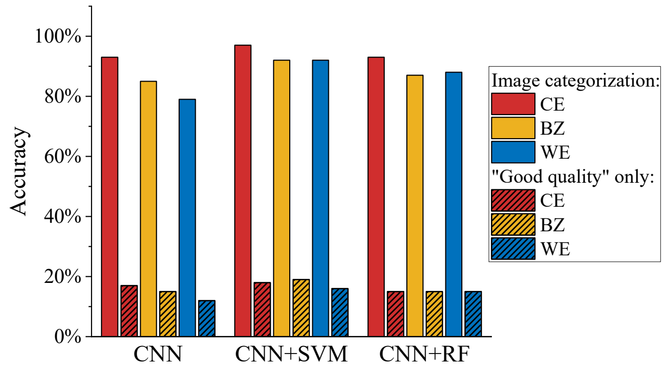


**Figure 6.** Accuracy of discharge classification of images under environmental disturbances. Bars with and without patterns show the results using the models trained with only "Good quality" samples and samples after automated image categorization, respectively. Color enhancement methods include Color Enhanced (CE), Binarization (BZ), and Water-color Enhanced (WE).

### 3.3.2 Comparison of models and color-enhancing methods

The stream image samples after the treatments of color-enhancing, image denoising, and automated image categorization were randomly divided into training and validation sets by the ratio of 7:3. The scatter plots of measured and simulated discharge based on the validation samples (**Fig. 7**) show that all three models (i.e., CNN, CNN+SVM, CNN+RF) can achieve satisfactory accuracy. The simulated discharges were all significantly correlated to the flowmeters' measurement with *R* values higher than 0.95. The observed and simulated discharge under most flow conditions were distributed around the 1:1 line with *RMSE* of 1.39, 1.02, and 0.69 $dm^3/s$, respectively. However, a comparison of the three models suggests that CNN is more likely to over- or under-

https://doi.org/10.5194/egusphere-2023-659
Preprint. Discussion started: 5 May 2023


estimate discharge than both CNN+SVM and CNN+RF. CNN+RF achieved the best fit with the lowest *RMSE*. On the other hand, CNN+SVM shows the best performance on discharge classification (**Fig. 8**) with an accuracy higher than 91.3% using all three color-enhancing methods, which was 13.2%-14.4% higher than CNN and 2.2%-4.2% higher than CNN+RF. Such results could be related to the size of our samples and the characteristic of the features extracted by deep layers of CNN. SVM has been widely used for its capability to solve classification problems in the cases of small samples with linear features. It uses slack variables to allow the distances to the classification plane not to meet the original requirements for some points, thus avoiding overfitting in the training period.

Among the three tested color-enhancing methods, the Color Enhanced approach generally shows the best adaptability with the discharge classification models, with an accuracy 2.5%-5.2% higher than the Binarization and Water-color Enhanced images of the validation set. This may be caused by the different treatments in the edges of the water body. Binarization and Water-color Enhanced relatively cause larger deviation from the real edges, while Color Enhanced retains the image information to the maximum extent so that CNN can automatically and accurately identify the color differences between the target water body and the background. Overall, CNN+SVM using samples processed by the automated image categorization and Color Enhanced procedures performs best with a classification accuracy of 94.7%.

https://doi.org/10.5194/egusphere-2023-659
Preprint. Discussion started: 5 May 2023


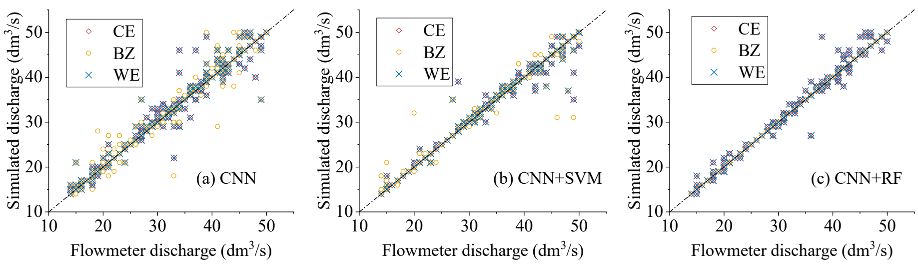


**Figure 7**. Comparison of discharge simulated from the validation set's images and the flowmeters' measurement. The used deep learning models include CNN (a), CNN+SVM (b), and CNN+RF (c). Color enhancement methods include Color Enhanced (CE), Binarization (BZ), and Water-color Enhanced (WE).

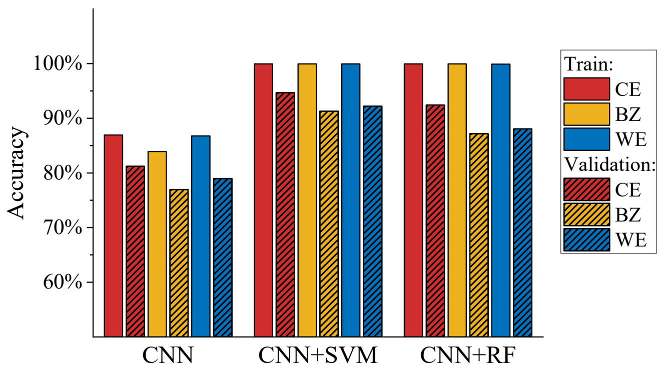


**Figure 8.** Accuracy of discharge classification on the training (bars without patterns) and validation set (bars with patterns). Color enhancement methods include Color Enhanced (CE), Binarization (BZ), and Water-color Enhanced (WE).

## 4 Discussion

The existing image-based methods usually rely on either the estimations of flow velocity and cross-section area or assumptions on stage-discharge correlation (Davids

https://doi.org/10.5194/egusphere-2023-659
Preprint. Discussion started: 5 May 2023


et al., 2019; Leduc et al., 2018; Li et al., 2019; Tauro et al., 2017). The first type of method uses image-derived surface velocity to estimate sub-sectional mean streamflow velocity and spatial integration of discharge (Le Coz et al., 2012). The difficulties in capturing cross-sectional characteristics and the relationship between flow velocity and water depth limit their application in small mountain streams. The second type of method retrieves river geometry directly through remote sensing, yet the accuracy is primarily determined by the empirical assumptions on the relationships among water depth, velocity, and discharge (Gleason and Smith, 2014; Young et al., 2015). In this study, we proposed a new camera-based method to directly establish the relationship between the RGB matrixes of stream images and the classification probabilities of discharge. The unique merit of the CNN-based model is its capability in automatically extracting and refining discharge-related features from image samples, which improves the accuracy and applicability of the model. Previous attempts suggest that the selection of image features can significantly affect the performance on classification of stream images (Tauro et al., 2014). For example, Chapman et al. (2020) manually extracted features from pre- and post-weir images and used them as the inputs of machine learning models. However, the dominant image features relating to stream discharge could vary across different environments (e.g., topography, vegetation on river banks, water quality), limiting the transferability of such manually identified features.

Weather conditions (e.g., sun position, fog, rain) are the most common difficulties that reduce picture quality (Leduc et al., 2018). Therefore, we designed an automated procedure for categorizing samples by their brightness and saturation: (a) select four

https://doi.org/10.5194/egusphere-2023-659
Preprint. Discussion started: 5 May 2023


areas in the image as detection areas, (b) eliminate images with insufficient light or raindrops on the lens, (c) identify thresholds and classify the remaining images into four categories for further model training, including the images under the influence of vegetation shadow and overexposure caused by water reflection in certain angles. Such inclusion and categorization of defective samples have significantly enhanced the anti-interference ability of the model, facilitating uninterrupted discharge monitoring through the daytime. These factors and the thresholds of brightness and saturation are site-specific and require manual trials to identify them. However, after adequate initial calibration, an established model can be used for the same site for extended periods and repeated installations of camera systems.

The training and validation of deep learning models require a large number of representative samples (He et al., 2016). We collected a total of 7757 image samples from July 20$^{th}$ to September 27$^{th}$, 2022, and 3464 images were used for model training and validation after image screening and categorization. Although we executed an effective automatic categorization procedure on the acquired image samples, it is undeniable that the training and validation sets didn't cover all environmental disturbances. For example, the time of sunrise and sunset, the appearance of water surface reflections, and the coverage of vegetation shadows are affected by the angles of sunlight and vary with seasons. With sufficient artificial lighting or installation of a night-vision infrared camera (Royem et al., 2012), the images during nighttime can also be used for discharge monitoring after training. More image samples are needed to enrich the representativeness of the model in further studies. Another limitation is that we have focused on low and average flow conditions in the model training due to the lack of high-quality flood samples. In tropical and subtropical mountain streams of southern China, floods usually occur during rainstorms and only last for a short time. Heavy rainfalls constantly block the camera lens with raindrops, and the rapid streamflow movement during heavy rainfall tends to cause blurred images, which can only be partly improved by increasing the shutter speed and adjusting the camera position.

## 5 Conclusions

The results demonstrate the effectiveness of a novel method for discharge monitoring of mountain streams using deep learning and a low-cost solar-powered commercial camera (approximately $200). The discharge-relevant stream features embedded in a large number of RGB images can be implicitly recognized and retrieved by CNN to achieve continuous discharge monitoring. Coupling CNN and traditional machine learning methods can potentially improve model performance in discharge classification to various extents. In this case, the accuracy of CNN+SVM and CNN+RF were 9.1%-14.4% higher than CNN. Proper image pre-processing and categorization can largely enhance the applicability of image-based discharge monitoring. In an environment under complex disturbances such as mountain streams, image quality is constantly interfered with by shadows of vegetation on the river banks. The automated image categorization procedure can effectively recognize discharge from defective

https://doi.org/10.5194/egusphere-2023-659
Preprint. Discussion started: 5 May 2023


images by filtering samples under different conditions and improve model robustness. The comparison of the three color-enhancing approaches also confirms the importance of including the non-water parts (e.g., large rocks) and retaining the background information to the maximum extent in the image analysis.

The proposed method provides an inexpensive and flexible alternative apparatus for continuous discharge monitoring at rocky upstream mountain streams, where it is challenging to identify the cross-section shape or establish a stable stage-discharge relationship. Site-specific field data is needed to identify the criteria for image categorization and model validation. However, it circumvents the potential errors in assuming cross-section characteristics, such as the relationship between water depth and flow velocity, and represents a new direction for applying deep learning techniques in acquiring high-frequency discharge data through image analysis.

## Code/Data availability

The code and data are available upon request from the corresponding author.

## Author contribution

KD and CF conceptualized the experiments. GY, ZZ, and QZ curated the data. All authors participated in the investigation. CF, GY, ZZ, and QZ wrote the original draft and visualized the data. KD reviewed and edited the final version of the manuscript.

https://doi.org/10.5194/egusphere-2023-659
Preprint. Discussion started: 5 May 2023


## Competing interests

The authors declare no competing interests.

## Acknowledgments

This work was supported by the National Key Research and Development Program of China (2021YFC3200205, 2021YFC3001000), the National Natural Science Foundation of China (51909285), the Guangdong Provincial Department of Science and Technology (2019ZT08G090), and the Guangdong Natural Science Foundation (2023A1515012241).

## References

Abdullah-Al-Wadud, M., Kabir, M. H., Dewan, M. A. A., and Chae, O.: A dynamic histogram equalization for image contrast enhancement, IEEE transactions on consumer electronics, 53, 593-600, 2007.

Aslam, J. A., Popa, R. A., and Rivest, R. L.: On Estimating the Size and Confidence of a Statistical Audit, EVT, 7, 8, 2007.

Breiman, L.: Random forests, Machine learning, 45, 5-32, 2001.

Burges, C. J.: A tutorial on support vector machines for pattern recognition, Data mining and knowledge discovery, 2, 121-167, 1998.

Carlisle, D. M., Grantham, T. E., Eng, K., and Wolock, D. M.: Biological relevance of streamflow metrics: regional and national perspectives, 36, 927-940, 10.1086/694913, 2017.

Chang, F., Hong, W., Zhang, T., Jing, J., and Liu, X.: Research on wavelet denoising for pulse signal based on improved wavelet thresholding, 2010 First International Conference on Pervasive Computing, Signal Processing and Applications, 564-567,

https://doi.org/10.5194/egusphere-2023-659
Preprint. Discussion started: 5 May 2023


10.1109/PCSPA.2010.142, 2010.

Chapman, K. W., Gilmore, T. E., Chapman, C. D., Mehrubeoglu, M., and Mittelstet, A. R.: Camera-based Water Stage and Discharge Prediction with Machine Learning, Hydrol. Earth Syst. Sci. Discuss., 2020, 1-28, 10.5194/hess-2020-575, 2020.

Cheng, H.-D. and Shi, X.: A simple and effective histogram equalization approach to image enhancement, Digital signal processing, 14, 158-170, 2004.

Clarke, R. T.: Uncertainty in the estimation of mean annual flood due to rating-curve indefinition, Journal of Hydrology, 222, 185-190, https://doi.org/10.1016/S0022-1694(99)00097-9, 1999.

Cortes, C. and Vapnik, V.: Support-vector networks, Machine learning, 20, 273-297, 1995.

Council, N. R.: Assessing the National Streamflow Information Program, The National Academies Press, Washington, DC, 176 pp., doi:10.17226/10967, 2004.

Czuba, J. A., Foufoula-Georgiou, E., Gran, K. B., Belmont, P., and Wilcock, P. R.: Interplay between spatially explicit sediment sourcing, hierarchical river-network structure, and in-channel bed material sediment transport and storage dynamics, 122, 1090-1120, https://doi.org/10.1002/2016JF003965, 2017.

Davids, J. C., Rutten, M. M., Pandey, A., Devkota, N., van Oyen, W. D., Prajapati, R., and van de Giesen, N.: Citizen science flow – an assessment of simple streamflow measurement methods, Hydrology and Earth System Sciences, 23, 1045-1065, 10.5194/hess-23-1045-2019, 2019.

DeWeber, J. T., Tsang, Y.-P., Krueger, D., Whittier, J. B., Wagner, T., Infante, D. M., and Fisheries, G. W. J.: Importance of Understanding Landscape Biases in USGS Gage Locations: Implications and Solutions for Managers, 39, 155-163, 2014.

Finlayson, G. D., Hordley, S. D., and Drew, M. S.: Removing shadows from images, Computer Vision—ECCV 2002: 7th European Conference on Computer Vision Copenhagen, Denmark, May 28–31, 2002 Proceedings, Part IV 7, 823-836, 2002.

Fujita, I., Muste, M., and Kruger, A.: Large-scale particle image velocimetry for flow analysis in hydraulic engineering applications, Journal of hydraulic Research, 36, 397-414, 1998.

Fujita, I., Watanabe, H., and Tsubaki, R.: Development of a non-intrusive and efficient flow monitoring technique: The space-time image velocimetry (STIV), International Journal of River Basin Management, 5, 105-114, 10.1080/15715124.2007.9635310, 2007.

Gershon, R., Jepson, A. D., and Tsotsos, J. K.: Ambient illumination and the determination of material changes, JOSA A, 3, 1700-1707, 1986.

Gleason, C. J. and Smith, L. C.: Toward global mapping of river discharge using satellite images and at-many-stations hydraulic geometry, Proc Natl Acad Sci U S A, 111, 4788-4791, 10.1073/pnas.1317606111, 2014.

Hanczar, B., Hua, J., Sima, C., Weinstein, J., Bittner, M., and Dougherty, E. R.: Small-sample precision of ROC-related estimates, Bioinformatics, 26, 822-830, 2010.

Hannah, D. M., Demuth, S., van Lanen, H. A., Looser, U., Prudhomme, C., Rees, G., Stahl, K., and Tallaksen, L. M.: Large-scale river flow archives: importance, current status and future needs, Hydrological Processes, 25, 1191-1200, 2011.

He, K., Zhang, X., Ren, S., and Sun, J.: Deep residual learning for image recognition, Proceedings of the IEEE conference on computer vision and pattern recognition, 770-778, 2016.

Herzog, A., Stahl, K., Blauhut, V., and Weiler, M.: Measuring zero water level in stream reaches: A comparison of an image-based versus a conventional method, Hydrological Processes, 36, 10.1002/hyp.14658, 2022.

Ho, T. K.: Random decision forests, Proceedings of 3rd international conference on document analysis and recognition, 278-282, 1995.

Karvonen, J.: Virtual radar ice buoys – a method for measuring fine-scale sea ice drift, The Cryosphere, 10, 29-42, 10.5194/tc-10-29-2016, 2016.

Kasuga, K., Hachiya, H., and Kinosita, T.: Quantitative Estimation of the Ultrasound Transmission Characteristics for River Flow Measurement during a Flood, Japanese Journal of Applied Physics, 42, 3212, 10.1143/JJAP.42.3212, 2003.

Kim, W., Roh, S.-H., Moon, Y., and Jung, S.: Evaluation of RedEdge-M camera for

https://doi.org/10.5194/egusphere-2023-659
Preprint. Discussion started: 5 May 2023


water color observation after image preprocessing, Journal of the Korean Society of Surveying, Geodesy, Photogrammetry and Cartography, 37, 167-175, 2019.

Krizhevsky, A., Sutskever, I., and Hinton, G. E.: Imagenet classification with deep convolutional neural networks, Communications of the ACM, 60, 84-90, 2017.

Le Coz, J., Camenen, B., Peyrard, X., and Dramais, G.: Uncertainty in open-channel discharges measured with the velocity–area method, Flow Measurement and Instrumentation, 26, 18-29, 2012.

LeCun, Y., Bengio, Y., and Hinton, G.: Deep learning, nature, 521, 436-444, 2015.

Leduc, P., Ashmore, P., and Sjogren, D.: Stage and water width measurement of a mountain stream using a simple time-lapse camera, Hydrology and Earth System Sciences, 22, 1-11, 2018.

Li, W., Liao, Q., and Ran, Q.: Stereo-imaging LSPIV (SI-LSPIV) for 3D water surface reconstruction and discharge measurement in mountain river flows, Journal of Hydrology, 578, 10.1016/j.jhydrol.2019.124099, 2019.

Matykiewicz, P. and Pestian, J.: Effect of small sample size on text categorization with support vector machines, BioNLP: Proceedings of the 2012 Workshop on Biomedical Natural Language Processing, 193-201,

McMillan, H., Freer, J., Pappenberger, F., Krueger, T., and Clark, M.: Impacts of uncertain river flow data on rainfall-runoff model calibration and discharge predictions, 24, 1270-1284, https://doi.org/10.1002/hyp.7587, 2010.

Noto, S., Tauro, F., Petroselli, A., Apollonio, C., Botter, G., and Grimaldi, S.: Low-cost stage-camera system for continuous water-level monitoring in ephemeral streams, Hydrological Sciences Journal, 67, 1439-1448, 10.1080/02626667.2022.2079415, 2022.

Panda, B., Herbach, J. S., Basu, S., and Bayardo, R. J.: Planet: massively parallel learning of tree ensembles with mapreduce, 2009.

Royem, A., Mui, C., Fuka, D., and Walter, M.: Proposing a low-tech, affordable, accurate stream stage monitoring system, Transactions of the ASABE, 55, 2237-2242, 2012.

https://doi.org/10.5194/egusphere-2023-659
Preprint. Discussion started: 5 May 2023


Sauvola, J. and Pietikäinen, M.: Adaptive document image binarization, Pattern recognition, 33, 225-236, 2000.

Tauro, F., Grimaldi, S., and Porfiri, M.: Unraveling flow patterns through nonlinear manifold learning, PloS one, 9, e91131, 2014.

Tauro, F., Piscopia, R., and Grimaldi, S.: Streamflow Observations From Cameras: Large-Scale Particle Image Velocimetry or Particle Tracking Velocimetry?, Water Resources Research, 53, 10374-10394, https://doi.org/10.1002/2017WR020848, 2017.

Tauro, F., Tosi, F., Mattoccia, S., Toth, E., Piscopia, R., and Grimaldi, S.: Optical Tracking Velocimetry (OTV): Leveraging Optical Flow and Trajectory-Based Filtering for Surface Streamflow Observations, Remote Sensing, 10, 10.3390/rs10122010, 2018.

Tsubaki, R.: On the Texture Angle Detection Used in Space-Time Image Velocimetry (STIV), Water Resources Research, 53, 10908-10914, 10.1002/2017wr021913, 2017.

Yorke, T. H. and Oberg, K. A.: Measuring river velocity and discharge with acoustic Doppler profilers, Flow Measurement and Instrumentation, 13, 191-195, https://doi.org/10.1016/S0955-5986(02)00051-1, 2002.

Young, D. S., Hart, J. K., and Martinez, K.: Image analysis techniques to estimate river discharge using time-lapse cameras in remote locations, Computers & Geosciences, 76, 1-10, 10.1016/j.cageo.2014.11.008, 2015.

Zhang, D.: Wavelet transform. Cham, Fundamentals of Image Data Mining, 35-44, 2019.